Thermal and Optical Switching of Molecular Spin States in the {[FeL[$H_2B(pz)_2$]$_2$]$_2$} Spin-Crossover System (L = bpy, phen)†

Nicolás Moliner,[1a] Lionel Salmon,[1b] Laurence Capes,[1c] M. Carmen Muñoz,[1d] Jean-François Létard,[1c] Azzedine Bousseksou,*[,1b] Jean-Pierre Tuchagues,[1b] John J. McGarvey,[1e] Andrew C. Dennis,[‡,1e] Miguel Castro,[1f] Ramón Burriel,[1f] and José Antonio Real*[,1a]

Departament de Química Inorgánica/Institut de Ciencia Molecular, Universitat de València, Dr. Moliner 50, E-46100 Burjassot, València, Spain, Groupe des Sciences Moléculaires, Institut de Chimie de la Matière Condensée de Bordeaux, UPR 9048 CNRS, 33608 Pessac, France, Laboratoire de Chimie de Coordination du CNRS, 205 route de Narbonne, 31077 Toulouse, France, Departament de Física Aplicada, Universitat Politècnica de València, Camino de Vera s/n, 46071, València, Spain, School of Chemistry, The Queen's University of Belfast, Belfast BT9 5AG, N. Ireland, and Instituto de Ciencia de Materiales de Aragón, CSIC-Universidad de Zaragoza, 50009 Zaragoza, Spain

Received: October 17, 2001

Mössbauer and Raman spectroscopies, calorimetric measurements, the LIESST effect (light induced excited spin state trapping) and dynamics of the high-spin (HS) to low-spin (LS) relaxation have been investigated in order to thoroughly study the spin-crossover compounds of formula {Fe(L)[$H_2B(pz)_2$]$_2$}, where L = 2,2′-bipyridine (**1**) and 1,10-phenanthroline (**2**). The Mössbauer studies have revealed the occurrence of an almost complete spin conversion at low temperature, while 9.5% (**1**) and 15% (**2**) of molecules remain LS at room temperature. The thermal variation of the proportion of HS molecules, n_{HS}, obtained from the Mössbauer spectra has been used to calibrate the thermal dependence of n_{HS} deduced from the magnetic susceptibility measurements. The thermodynamic Slichter and Drickamer model was used to fit the thermal variation of n_{HS}. The estimated thermodynamic parameters are $\Delta H = 7.7$ kJ mol^{-1}, $\Delta S = 47.4$ J mol^{-1} K^{-1} and interaction parameter $\Gamma = 2.1$ kJ mol^{-1} for **1** and $\Delta H = 7.9$ kJ mol^{-1}, $\Delta S = 48.3$ J mol^{-1} K^{-1} and $\Gamma = 3$ kJ mol^{-1} for **2**. These data agree with those obtained from heat capacity experiments: $\Delta H = 7.7 \pm 0.4$ kJ mol^{-1} and $\Delta S = 48 \pm 3$ J mol^{-1} K^{-1} for **1**, and $\Delta H = 8.0 \pm 0.4$ kJ mol^{-1} and $\Delta S = 49 \pm 3$ J mol^{-1} K^{-1} for **2**. The transition temperatures, estimated from the heat capacity peaks, were $T_c = 159.5$ K for **1**, and T_c(up) = 165.0 K, T_c(down) = 162.7 K for **2**, in heating and cooling processes. Raman spectra have been recorded for **2** both in the HS (300 K) and LS (110 K) states. Significant changes occur in the position of several low-frequency Raman modes in the low-temperature spectrum. The entropy change associated with the 15 normal vibrational modes of the [FeN_6] pseudo-octahedron has been estimated from the measured spectra as $\Delta S_{vib} = 36$ J K^{-1} mol^{-1}, and the total entropy change is $\Delta S = \Delta S_{vib} + \Delta S_{el} = 49$ J K^{-1} mol^{-1}. This value is comparable to that obtained from the calorimetric measurements. Photomagnetic studies revealed a complete conversion from the LS into the HS state upon irradiation at 10 K in the 647.1−676.4 nm wavelength region. The critical LIESST temperatures are 52 K (**1**) and 44 K (**2**). The dynamics of the LS to HS conversion was studied for the two compounds in the 6−50 K temperature range. In the thermally activated region the apparent activation energy, E_a, was estimated to be 240 cm^{-1} for **1** and 170 cm^{-1} for **2**. In the tunneling region the rate constants were estimated to lie in the 9×10^{-7} to 1×10^{-6} s^{-1} range.

Introduction

Functional materials made up from discrete molecules represent an increasingly important area of investigation in contemporary chemistry.[2] Functionality depends on the electronic structure of the constituent molecules. For instance, switchable molecules have the ability to occur in two different long-lived states. Switching between two states may induce drastic changes in chemical and physical properties of the molecule, and hence of the material.

Six-coordinate Fe(II) spin-crossover compounds represent an important class of switchable molecular systems. They change reversibly from a low-spin (LS) diamagnetic state at low temperatures to a high-spin (HS) paramagnetic state at higher temperatures. This phenomenon is observed both in solution and in the solid state. In solution the process is essentially molecular because the molecules are isolated, whereas cooperative intermolecular interactions leading to first-order spin transitions may be observed in the solid state. Cooperativity stems from the large difference in metal−ligand bond length (ca. 0.2 Å) and the concomitant difference in volume of the molecules undergoing spin change.[3−5]

The primary driving force governing the spin conversion is the entropy increase associated with the LS ↔ HS conversion. This entropy change can be mainly ascribed to differences in

† Dedicated to the memory of Professor Olivier Kahn.

‡ Present address: Avalon Instruments Ltd., 10 Malone Road, Belfast BT9 5BN, N. Ireland.

10.1021/jp013872b CCC: $22.00
Published on Web 03/30/2002

spin multiplicity and in density of vibrational states associated with the LS and HS states.[6]

The spin-crossover phenomenon can be considered as a monomolecular intra-ionic two-electron-transfer process. Addressing spin states through light irradiation has represented an important stimulus in the study of the LS ↔ HS kinetics as well as for the comprehension of the dynamic mechanism of the spin-conversion.[7−11] On the other hand optical addressing has opened perspectives for optical switching and magnetooptical storage devices.[12]

In a recent paper we have reported the synthesis, X-ray structures, and magnetic properties of the {[FeL[$H_2B(pz)_2]_2$} systems ($H_2B(pz)_2^-$ = dihydrobis(pyrazolyl)borate, L = 2,2′-bipyridine (bpy) (**1**), and 1,10-phenanthroline (phen) (**2**)).[13] Magnetic measurements of **2** revealed the occurrence of a cooperative spin transition with a 4 K hysteresis loop and T_c(up) = 166 K and T_c(down) = 162 K for warming and cooling modes, respectively. For the bpy derivative, a more gradual spin conversion with T_c = 160 K was observed. In the present paper, we report the thermodynamic and kinetic studies of both spin conversions by means of Mössbauer and Raman spectroscopies, calorimetric measurements, photomagnetic (LIESST) experiments, and HS → LS relaxation studies.

Experimental Section

Preparation of the Samples. The syntheses of compounds **1** and **2** have been described elsewhere.[13] The elemental analyses data for **1** and **2** agree well with the calculated values.

Mössbauer Spectra. The variable-temperature Mössbauer measurements were obtained on a constant acceleration conventional spectrometer with a 50 mCi source of ^{57}Co (Rh matrix). Isomer shift values (δ) are given with respect to metallic Fe at room temperature. The absorber was a sample of about 100 mg of microcrystalline powder of **1** or **2** enclosed in a 2 cm diameter cylindrical plastic sample holder, the size of which had been determined to optimize the absorption. Variable-temperature spectra were obtained in the 305−4.2 K range, by using a MD306 Oxford cryostat, the thermal scanning being monitored by an Oxford ITC4 servo-control device (±0.1 K accuracy). A least-squares computer program[14] was used to fit the Mössbauer parameters and determine their standard deviations of statistical origin (given in parentheses).

Differential Scanning Calorimetry (DSC). Calorimetric measurements have been performed on **1** and **2** using a differential scanning calorimeter Perkin-Elmer DSC-7. Low temperatures were obtained with an aluminum block attached to the sample holder, refrigerated with a flow of liquid nitrogen and stabilized at a temperature of 110 K. The sample holder was kept in a drybox under a flow of dry nitrogen gas to avoid water condensation. The measurements were carried out using around 10 mg of powdered samples sealed in aluminum pans with a mechanical crimp. Temperature and enthalpy calibrations were made with standard samples of cyclohexane by using its melting (279.69 K, 2630 J mol^{-1}) and crystal to crystal transitions (186.10 K, 6698 J mol^{-1}). An overall accuracy of ±0.2 K in temperature and ±2% in the heat capacity is estimated. The uncertainty increases for the determination of the anomalous enthalpy and entropy due to the subtraction of an unknown baseline.

Raman Spectra. Raman spectra were excited at 785 nm using a Ti-sapphire laser pumped by an Ar^+ laser (Spectra Physics Model 2025).[15] Spectra were recorded by means of a liquid N_2 cooled CCD detector (Princeton Instruments, LN/UV 1152) coupled to Jobin-Yvon spectrograph Model HR640 with a 300 grooves mm^{-1} holographic grating. A 785 nm notch filter Kaiser Optics) was located in front of the spectrograph slit. A slit width of 100 μm was used for recording all spectra, with accumulation times of 4 × 10 s and a beam power of 20 mW at the sample.

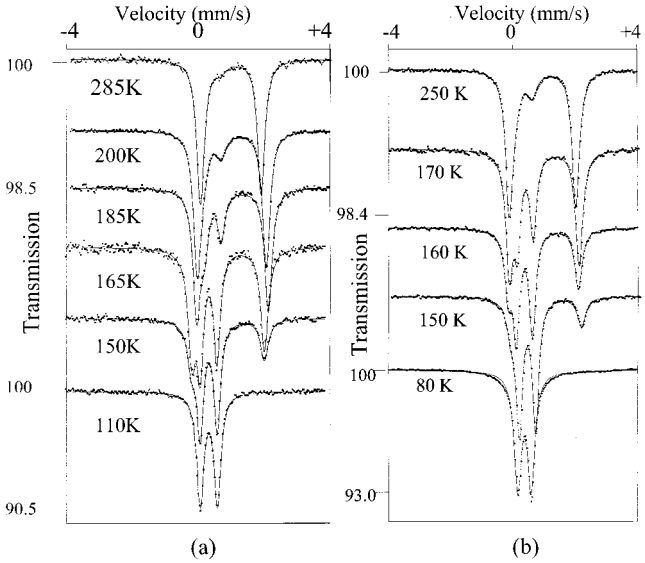

Figure 1. Selected Mössbauer spectra of **1** (a) and **2** (b) obtained in the cooling mode. The solid lines represent fitted curves.

Following the experimental setup described in ref 20, the pure microcrystalline powder sample was enclosed in an 18 mm diameter cylindrical aluminum holder and rotated during spectral acquisition. A simple liquid nitrogen cryostat of in-house design, with helium exchange gas was used for the studies at low temperature (110 K).

Photomagnetic Experiments. The LIESST experiments were performed by using a Spectra-Physics series 2025 Kr^+ laser system coupled to the cavity of a MPMS-55 Quantum Design SQUID magnetometer through an optical fiber. The measurements were performed on a very thin layer of powdered sample. The weight was estimated by comparing the thermally induced spin transition curve with the curve recorded with a heavier and accurately weighted sample. The critical LIESST temperatures were recorded at a temperature increase of 0.3 K min^{-1}. Irradiation was carried out using the multiline, 647.1 and 676.4 nm, of a Kr^+ laser. The power was adjusted to 10 mW/cm^2.

Results

Mössbauer Data. The temperature dependence of the ^{57}Fe Mössbauer spectra has been studied, for the bpy (**1**) and phen (**2**) derivatives, between 80 and 300 K. Figure 1 shows selected spectra obtained in the cooling mode. Detailed values of the Mössbauer parameters resulting from least-squares fitting procedures are listed in Table 1 for a representative set of temperatures. The main doublet observed at 285 K (**1**) and 250 K (**2**) is characterized by quadrupole splitting values of ΔE_q = 1.802(2) (**1**) and 1.953(2) (**2**) mm s^{-1} and isomer shift values of δ = 1.002(1) (**1**) and 1.030(2) (**2**) mm s^{-1}. These values are characteristic of the HS state of Fe(II). As the temperature is lowered, another doublet appears, whose intensity increases at the expense of the first one. The fitted parameters at 80 K are ΔE_q = 0.507(1) (**1**) and 0.505(1) (**2**) mm s^{-1} and δ = 0.514(1) (**1**) and 0.525(1) (**2**) mm s^{-1}. They are typical of the LS state of Fe(II). At 80 K, no residual HS species are detected. At 250 K, the temperature for which the spin crossover is supposed to be completed, the spectra indicate the presence of ca. 9.5% (**1**) and 15% (**2**) of LS species. No spectrum deformation or line

TABLE 1: ^{57}Fe Mössbauer Parameter for 1 and 2

	low-spin state			high-spin state			
T (K)	δ (mm s^{-1})	ΔE_Q (mm s^{-1})	$\Gamma/2$ (mm s^{-1})	δ (mm s^{-1})	ΔE_Q (mm s^{-1})	$\Gamma/2$ (mm s^{-1})	A_{HS}/A_{tot} (%)
			Compound **1**				
285	0.430(2)	0.510(5)	0.190(2)	1.002(1)	1.802(2)	0.128(2)	90.5(6)
200	0.475(3)	0.515(5)	0.168(4)	1.057(1)	2.049(1)	0.135(1)	84.2(3)
190	0.481(3)	0.493(5)	0.133(3)	1.069(1)	2.094(1)	0.131(1)	81.5(3)
180	0.485(2)	0.491(4)	0.127(3)	1.079(1)	2.125(1)	0.134(1)	74.4(4)
170	0.496(1)	0.496(2)	0.123(1)	1.077(1)	2.140(1)	0.135(1)	60.4(3)
165	0.496(1)	0.497(3)	0.118(2)	1.081(2)	2.151(3)	0.139(3)	52.4(6)
160	0.501(1)	0.501(1)	0.120(1)	1.080(1)	2.162(2)	0.137(1)	40.3(3)
155	0.505(1)	0.503(1)	0.121(1)	1.087(2)	2.156(1)	0.145(3)	31.2(5)
150	0.503(1)	0.503(1)	0.120(1)	1.084(2)	2.172(4)	0.149(3)	22.4(4)
110	0.507(1)	0.508(1)	0.123(1)			0	
80	0.514(1)	0.507(2)	0.130(1)			0	
			Compound **2**				
250	0.456(3)	0.486(2)	0.170(4)	1.030(2)	1.953(3)	0.135(2)	85.1(3)
200	0.476(3)	0.500(2)	0.168(4)	1.058(2)	2.049(3)	0.135(2)	84.5(3)
170	0.497(2)	0.496(2)	0.123(2)	1.078(2)	2.140(2)	0.135(3)	83.3(2)
160	0.502(2)	0.501(3)	0.120(2)	1.081(2)	2.162(2)	0.137(1)	25.3(2)
150	0.504(2)	0.503(2)	0.120(2)	1.085(2)	2.172(2)	0.149(3)	09.7(3)
100	0.521(1)	0.502(1)	0.123(2)				0
80	0.525(1)	0.505(1)	0.125(2)				0

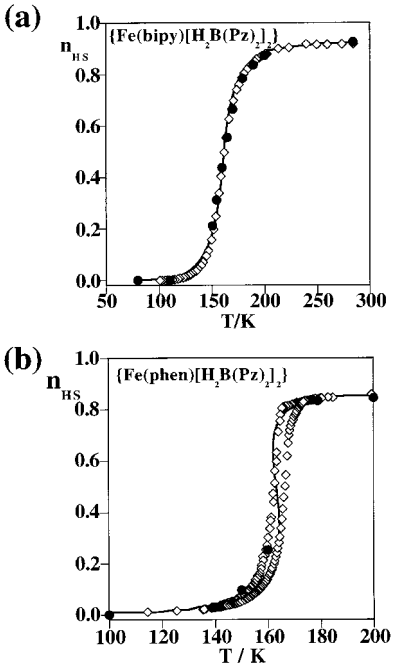

Figure 2. Thermal variation of the high-spin fraction, n_{HS}, of **1** (a) and **2** (b). Rhombuses and black circles represent the n_{HS} values deduced from magnetic susceptibility measurements and from Mössbauer spectroscopy data, respectively. The solid line represents a least-squares fit (see text).

broadening is observable in this temperature range, indicating that the spin-conversion rates are slow compared to the Mössbauer hyperfine frequencies (ca. 10^8s^{-1}).[16]

The thermal variation of the area ratio,

$$A_{HS}/A_{tot} \sim n_{HS} \tag{1}$$

where A_{tot} and A_{HS} are the total and the HS area of the Mössbauer spectra, respectively, and n_{HS} is the HS molar fraction, is shown in Figure 2. For complex **2**, the spin-crossover is abrupt with hysteresis. The thermal variation of n_{HS} obtained by Mössbauer spectroscopy is in perfect agreement with the n_{HS} values obtained from magnetic susceptibility (calibrated with Mössbauer data at 100 and 298 K where the spin conversion saturates, giving the LS and HS phases, respectively) (Figure 2b). In the case of complex **1**, for temperatures higher than 160 K, some deviation was observed between the curves obtained from magnetism (calibrated with Mössbauer data) and Mössbauer spectroscopy. In this case, the Mössbauer data have been corrected. The exact n_{HS} and n_{LS} fractions are proportional to the area of the HS and LS doublets (A_{HS} and A_{LS}) through

$$A_{HS} = \mathrm{ct} f_{HS} n_{HS} \tag{2}$$

$$A_{LS} = \mathrm{ct} f_{LS} n_{LS} \tag{3}$$

where ct is an instrumental constant for a determined sample, and f_{HS} and f_{LS} are the Lamb-Mössbauer resonant factors. By using expressions 1−3, we obtain the relationship between the Mössbauer area ratio (n'_{HS}) and the exact proportion (n_{HS}) of the HS state:

$$n_{HS} = [n'_{HS} f_{LS}]/[n'_{HS} f_{LS} + (1 - n'_{HS}) f_{HS}] \tag{4}$$

The thermal variation of $f_{LS,HS}$ has been deduced from the analysis of the total area of the spectra obtained for the overall 80−285 K temperature range in the Debye approximation, including a thickness correction using the formula:[17,18]

$$f_{LS,HS} = \exp[(-\alpha T)/\theta_D] \tag{5}$$

where α is a constant, being 136 K for ^{57}Fe, and θ_D is the Debye temperature. A subsequent study of the thermal variation of the recoil-free fraction of the system has been carried out through least-squares fitting procedures[19] of the total Mössbauer absorption, allowing one to obtain the Debye temperature for this complex: $\theta_{D,LS} = 136$ K and $\theta_{D,HS} = 130$ K in the LS and HS states, respectively. From the temperature dependence of ln(A_{tot}) (Figure S1, Supporting Information), derived from the above-mentioned measurements, we have obtained the temperature dependence of the actual proportion of HS molecules for **1**. As can be seen, the corrected $n_{HS}(T)$ curve (full circles in Figure 2) fits perfectly to the curve obtained from the magnetic data (calibrated by Mössbauer spectroscopy: open rhombuses).

DSC Measurements. The calorimetric measurements, recorded for heating and cooling rates of 10 K min^{-1}, were carried out in the 120−220 K temperature range. For each compound a smooth line has been interpolated from the values in the normal regions, below 140 K and above 190 K. The heat capacity due to the transition has been deduced by subtraction of this baseline. The temperature dependence of the anomalous

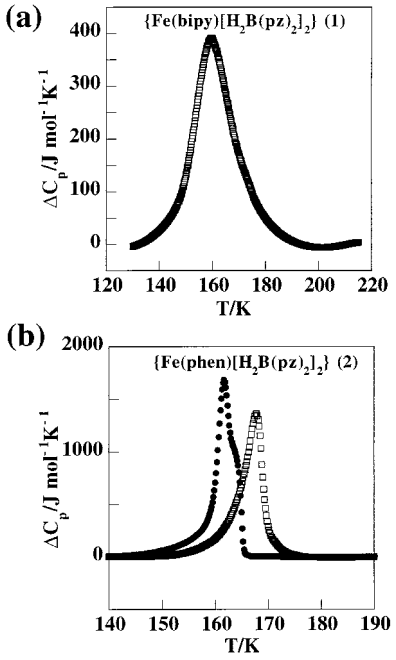

Figure 3. Calorimetric measurements of **1** (a) and **2** (b). Black circles and open squares represent calorimetric measurements in the cooling and warming modes for **2**, respectively.

heat capacity, ΔC_p, in the heating mode for **1** and in the heating and cooling modes for **2** are shown in Figure 3. The temperature of the maximum of the heat capacity curves were obtained for heating and cooling thermograms measured at different rates. The extrapolation at zero rate gave the same transition temperature on heating and cooling without any noticeable hysteresis for **1** and a hysteresis of 2.3 K for **2**. The critical temperature, T_c, has been obtained from the maximum of ΔC_p vs T, after correcting for the heating and cooling thermal lags. We found $T_c = 159.5$ K for **1**, T_c (down) = 162.7 K and T_c(up) = 165.0 K for **2**. These values agree rather well with those observed from the $\chi_M T$ vs T plots: $T_c = 159.8$ K for **1**, T_c (down) = 161.8 K and T_c(up) = 165.6 K. The enthalpy variation, ΔH, associated with the spin transition determined from the DSC curves is $\Delta H = 7.7 \pm 0.4$ kJ mol^{-1} (**1**) and 8.0 ± 0.4 kJ mol^{-1} (**2**). The overall entropy variation upon the spin transition, calculated by integration of the anomalous C_p/T over the spin conversion region, is $\Delta S = 48 \pm 3$ J mol^{-1} K^{-1} (**1**) and $\Delta S = 49 \pm 3$ J mol^{-1} K^{-1} (**2**).

Raman Spectroscopy. Figure 4 shows the Raman spectra obtained from a pure powder sample of **2** at room temperature (HS state) and 110 K (LS state) over the energy range 100−1800 cm^{-1}. Features in the spectral region below 100 cm^{-1} were excluded from consideration due to the nonlinear performance of the notch filter close to the Rayleigh line.

Well-defined spectral features observed in the high-energy region (1800−700 cm^{-1}), can be assigned to the phen and $H_2B(pz)_2^-$ ligands. Because of their smaller relative change with spin and their lower contribution to the entropy change, these vibrational modes will be neglected in the present analysis.[20,21]

The most significant changes in vibrational band frequencies appear in the range 100−650 cm^{-1}. Upon LS → HS conversion, the peaks below ca. 650 cm^{-1} undergo an overall shift to lower frequencies. In this type of coordinated compound the vibrational modes associated with the skeletal vibrations of the [FeN_6] pseudo-octahedral core are present in this region.[22] For a regular octahedron there are six internal modes with different degeneracies, only three of which are Raman active. In both spin states, the local symmetry of the [FeN_6] core is C_2, with an effective atomic arrangement close to C_{2v}. This symmetry lowering is accompanied by a total split of the degeneracies into 15 modes of the [FeN_6] core, and all of them are Raman active.

The observed frequency bands in the 100−650 cm^{-1} range have been considered representative of the fifteen internal vibrational modes of the [FeN_6] core. The same assumption was adopted recently in a similar Raman spectral analysis performed on the [$Fe(phen)_2(NCS)_2$] spin-crossover system.[20] This hypothesis has received some support from recent DFT calculations made on the [$Fe(phen)_2(NCS)_2$] compound.[23] There are nine clearly observed modes in the LS state below 650 cm^{-1}. On the assumption that the same symmetry is maintained in both spin states, the nine lowest energy modes in the HS state have also been considered. The frequency values observed at 110 and 300 K have been assigned to the LS and HS states at the transition temperature since they apparently do not change significantly with temperature. For the following vibrational features (cm^{-1}) assigned to the **LS** and **HS** states,

LS state (100 K): 303, 357, 389, 436, 470, 498, 589, 615, 640 cm^{-1},

HS state (300 K): 136, 189, 231, 253, 258, 277, 308, 410, 418 cm^{-1},

the entropy of each corresponding mode has been calculated from the expression derived for a harmonic oscillator of frequency ω,[20]

$$S(\omega_i,T) = \frac{\hbar\omega_i}{2T_c \tanh\left(\frac{\hbar\omega_i}{2kT_c}\right)} - k \ln\left[2 \sinh\left(\frac{\hbar\omega_i}{2kT_c}\right)\right] \qquad (6)$$

The vibrational entropy change for each mode is obtained from the expression

$$\Delta S_{vib}(\omega_i) = S_{HS}(\omega_i,T_c) - S_{LS}(\omega_i,T_c) \qquad (7)$$

where ω_i is the wave number corresponding to the ith vibrational mode. Figure 5 shows explicitly the total vibrational entropy change (15 modes for octahedral coordination) as a function of the geometric average of the vibrational frequencies in the high-spin state for different values of T_c and with a ratio $\omega_{av,LS}/\omega_{av,HS} = 1.78$ (a**)**, and for different values of the ratio $\omega_{av,LS}/\omega_{av,HS}$ and with $T_c = 163$ K (b). In the present case (compound **1**), the low-frequency approximation,[21,24] assuming that the contribution of all modes to the entropy change is the value at saturation of $\Delta S(\omega)$ (Figure 5b, small ω values), cannot be used because of the comparable energy values of kT_c and $\hbar\omega_i$ for the relevant frequencies.

The total ΔS_{vib} arising from the frequency change associated with the spin conversion has been calculated by multiplying the entropy difference for the nine observed modes by 15/9 to compensate for the unknown frequencies. The calculation with the exact expressions (6) and (7) used here happens to be only around 50% of the value given by the low-frequency approximation in this case.

Taking into account the additional entropy change from the electronic degeneracies of the spin states, the total entropy change is

$$\Delta S = \Delta S_{vib} + R \ln(g_{HS}/g_{LS}) \qquad (8)$$

where $g_{LS,HS} = (2S_{LS,HS} + 1)$ denotes the electronic degeneracies of the spin states, respectively**.** The calculated entropy of vibrational origin, $\Delta S_{vib} = 35.9$ J K^{-1} mol^{-1}, gives a total

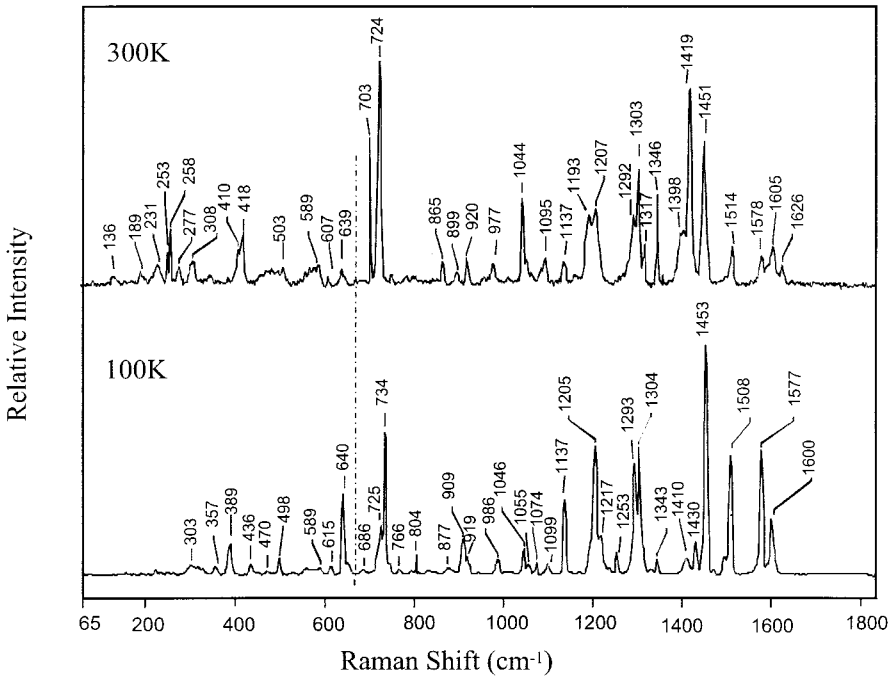

Figure 4. Raman spectra of **2** at two temperatures above and below T_c.

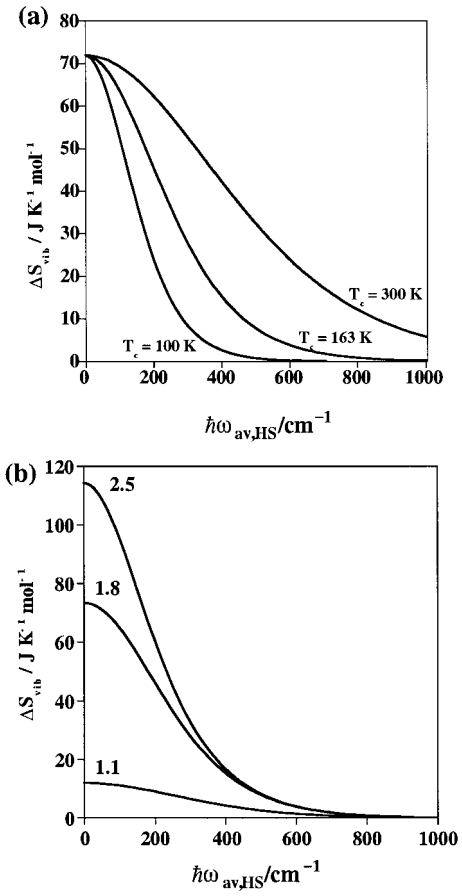

Figure 5. Calculated vibrational part of the entropy change upon spin crossover as a function of the average frequency of 15 vibrational modes for (a) different values of T_c and $\omega_{av,LS}/\omega_{av,HS} = 1.78$ and (b) $T_c = 163$ K and $\omega_{av,LS}/\omega_{av,HS} = 2.5$, 1.8, and 1.1. The present studied compound **2** corresponds to $T_c = 163$ K, $\omega_{av,LS} = 464$ cm^{-1}, and $\omega_{av,LS}/\omega_{av,HS} = 1.78$ cm^{-1}.

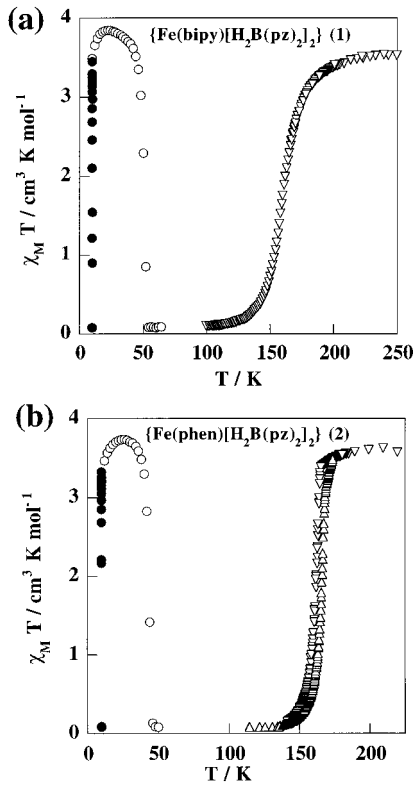

Figure 6. Temperature dependence of the $\chi_M T$ product for **1** (a) and **2** (b) (△); (●) data recorded with irradiation for 1 h at 10 K; (○) data recorded in the warming mode (0.3 K min^{-1}) after the light irradiation was turned off.

entropy change $\Delta S = 49.3$ J K^{-1} mol^{-1} at the spin crossover transition temperature.

Photomagnetic Measurements. The LIESST experiments were performed on **1** and **2** by using a Kr^+ laser locked in the 647.1−676.4 nm multiline mode. A similar procedure was used for the two powdered samples.[25,26] The compound was first slowly cooled from ca. 100 K to 10 K and the $\chi_M T$ versus T curve was recorded. At 10 K, the sample was irradiated for 1 h (Figure 6). The magnetic response of the sample increased rapidly before approaching near the saturation HS limiting value. This indicates a complete conversion of the LS state into the

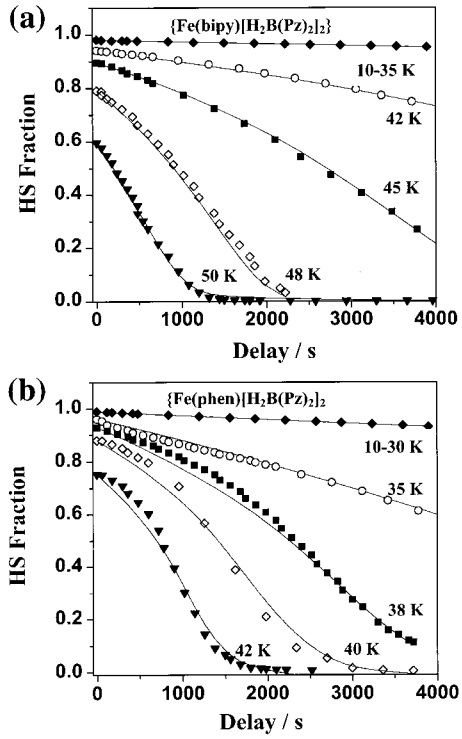

Figure 7. Time dependence at various temperatures of the HS molar fraction, n_{HS}, generated by light irradiation at 10 K.

HS state, according to the LIESST process.[8] The light irradiation was then turned off, and the temperature was increased at the rate of 0.3 K min^{-1}. $\chi_M T$ was found to remain in the HS state when the temperature is low enough, reaching the values 3.8 and 3.7 cm^3 K mol^{-1} for **1** and **2**, respectively, and then to drop rapidly within a temperature interval of a few kelvin. The critical LIESST temperature, $T_{c,LIESST}$,[26] was determined as the extreme of the $\partial(\chi_M T)/\partial T$ derivative. The $T_{c,LIESST}$ values are 52 K for **1** and 44 K for **2**.

The dynamics of the LIESST effect were studied for the two compounds from 10 K up to the highest temperature above which the relaxation becomes too fast for our SQUID setup. These upper-limit temperatures are 51 K (**1**) and 43 K (**2**). Figure 7 shows the decay of the HS molar fraction, n_{HS}, for the two compounds at various temperatures. In the 10−35 K temperature range the HS → LS relaxation is very slow. At 10 K the HS fraction varies about 4% within 12 h for both compounds. In contrast, around the $T_{c,LIESST}$ value, the dynamics of the HS → LS relaxation is fast. Such behavior is typical of spin-crossover compounds exhibiting LIESST properties.[8−10,27] The nearly temperature-independent relaxation behavior at low temperatures (LT region) and the thermally activated relaxation behavior at high temperatures (HT region) are interpreted according to the theory of nonadiabatic multiphonon relaxation.[28]

In the LT region, i.e., $T < 35$ K, the HS → LS relaxation is very slow and it is then difficult to accurately estimate the rate constant. From the kinetics recorded over a 12 h interval at 10 K, the rate constant of the tunneling region is calculated for both compounds to be in the range 9×10^{-7} to 1×10^{-6} s^{-1} by using a simple exponential analysis (eq 9).

Thermal activation of the relaxation process becomes more important in the HT region, i.e., $T \geq 35$ K. It is worth noting that the HS → LS relaxation curves show a strong deviation from single-exponential behavior. The n_{HS} curves can be reasonably well fitted to a sigmoidal-type behavior (eqs 9 and 10). Such sigmoidal relaxation curves have been previously

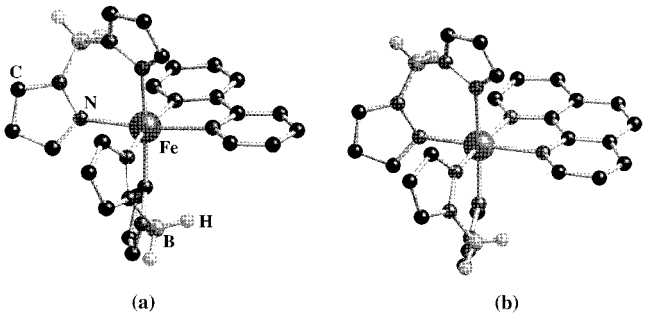

Figure 8. Perspective view of the molecular structures of **1** (a) and **2** (b).

TABLE 2: Rate Constants k_{HL} as a Function of Temperature T for 1 and 2

compounds[a]	T/K	k_{HL}/s^{-1}	$\alpha(T)$
{Fe(bpy)[$H_2B(pz)_2]_2$} (**1**)	35	7.5×10^{-6}	
	38	1.5×10^{-5}	5.4
	42	3.4×10^{-5}	4.1
	45	6.8×10^{-5}	3.5
	48	1.2×10^{-4}	3.6
	50	1.5×10^{-4}	3.6
	51	1.4×10^{-4}	3.6
{Fe(phen)[$H_2B(pz)_2]_2$} (**2**)	32	2.7×10^{-5}	
	35	6.1×10^{-5}	3.2
	36	8.1×10^{-5}	3.4
	38	9.3×10^{-5}	3.6
	40	1.2×10^{-4}	3.7
	42	1.5×10^{-4}	3.7
	43	1.8×10^{-4}	3.5

described for the pure $Fe(ptz)_6(BF_4)_2$ compound and attributed to cooperative effects.[11] Hauser has shown that the internal pressure associated with the large difference in metal−ligand bond lengths between HS and LS states induced both horizontal and vertical displacements of the two potential wells.[11] Consequently, the relaxation rate depends exponentially on both n_{LS} and T and on $\alpha(T)$, the acceleration factor at a given temperature.

$$\frac{\partial n_{LS}}{\partial t} = k^*_{HL}(1 - n_{LS}) \tag{9}$$

$$k^*_{HL}(T,n_{LS}) = k_{HL}(T)\exp[\alpha(T)n_{LS}] \tag{10}$$

A least-squares fit of the experimental data with $k_{HL}(T)$ and $\alpha(T)$ as free parameters is quite satisfactory. The resulting fit curves are shown in Figure 7. Table 2 collects the rate constant values k_{HL} estimated as a function of temperature. In the high-temperature region, the Arrhenius plot for the two compounds give some apparent straight lines with a preexponential factor $k_{HT} = 2 \times 10^{-1}$ s^{-1} for **1** (5×10^{-2} s^{-1} for **2**) and an activation energy $E_a = 240$ cm^{-1} for **1** (170 cm^{-1} for **2**). Nevertheless, these parameters are largely underestimated due to the tunneling process that prevails on thermal activation in the 30−50 K temperature range.

Discussion

The crystal structure of **1** and **2** have already been reported[13] and are sketched in Figure 8. Briefly, it can be noticed that the two compounds have similar pseudo-octahedral coordination cores. At room temperature, the mean Fe−[$H_2B(pz)_2^-$] bond distances are 2.171(2) Å and 2.173(3) Å for **1** and **2**, respectively. The average Fe−N(bpy, phen) bond distances are 2.213-(2) Å and 2.212(3) Å, respectively. Crystals of **2** cracked when cooled below T_c. In contrast, the crystal structure of the low-spin phase has been measured for **1**. The spin-transition mainly

affects the [FeN_6] core geometry, the Fe−N[$H_2B(pz)_2^-$] and Fe−N(bpy) bonds being shorter by 0.13 and 0.20 Å, respectively. The average variation in Fe to ligand bond distance is $\Delta r = 0.152$ Å.

The thermodynamic parameters ΔH and ΔS involved in the spin transition were estimated from the Slichter and Drickamer model[29] in the previous magnetic study.[13] These values were overestimated because the proportion of high-spin species was obtained from magnetic data without calibration by Mössbauer spectroscopy. The Mössbauer spectra have revealed the occurrence of 9.5% and 15% of LS species at room temperature for **1** and **2**, respectively. Consequently, the HS molar fraction, n_{HS}, derived from the magnetic susceptibility data[13] was calibrated with the n_{HS} ($\sim A_{HS}/A_{tot}$) value obtained at room temperature from the Mössbauer spectra. The solid line in Figure 2 represents the theoretical curve obtained by a least-squares fit of the n_{HS} variation with the macroscopic Slichter and Drickamer model,[29] formally equivalent to the other macroscopic models[21] and to the microscopic two-level Ising-like model.[24] The resulting parameters estimated with this model are $\Delta H = 7.7$ kJ mol^{-1}, $\Delta S = 47.4$ J. K^{-1} mol^{-1}, and $\Gamma = 2.1$ kJ mol^{-1} for **1**, and $\Delta H = 7.9$ kJ mol^{-1}, $\Delta S = 48.3$ J K^{-1} mol^{-1}, and $\Gamma = 3$ kJ mol^{-1} for **2**, Γ being an interaction parameter between the spin species.[29] These estimated values for the entropy and enthalpy variations fall within the limits obtained from the calorimetric measurements: $\Delta H = 7.7 \pm 0.4$ kJ mol^{-1} (**1**) and 8.0 ± 0.4 kJ mol^{-1} (**2**) and $\Delta S = 48 \pm 3$ J K^{-1} mol^{-1} (**1**) and 49 ± 3 J K^{-1} mol^{-1} (**2**).

As expected, ΔS values for **1** and **2** are significantly larger than the entropy variation resulting from the change in spin-only values ($\Delta S = R \ln[(2S_{HS} + 1)/(2S_{LS} + 1)] = 13.4$ J mol^{-1} K^{-1} for $S_{HS} = 2$ and $S_{LS} = 0$). The excess of entropy corresponds mainly to the changes associated with the intramolecular Fe−L bond lengths, ca. 0.2 Å shorter in the LS than in the HS state. The longer bond lengths of the HS state decrease the interatomic force constants, reducing the corresponding vibrational frequencies. As a result the number of excited vibrational states experience an abrupt jump with the lattice expansion. Consequently, the entropy increases at the transition temperature according to the expressions (6) and (7). The dominant contribution to the entropy arises from the softening of the metal−ligand skeletal vibrations on going from the LS to the HS state. The Raman spectra of **2** were recorded in order to investigate the contribution of the intramolecular vibrations to the increase in entropy upon spin-conversion. The resulting $\Delta S_{vib} = 35.9$ J K^{-1} mol^{-1} clearly represents a major contribution to the experimental value for the overall entropy change $\Delta S = 49.3$ J K^{-1} mol^{-1} (57 J K^{-1} mol^{-1} if we consider a complete spin conversion) and is significantly larger than the electronic contribution, $\Delta S_{elec} = 13.4$ J K^{-1} mol^{-1}. The excess experimental entropy over the calculated vibrational and electronic contributions, $\sim 57 - 35.9 - 13.4 = 7.7$ J K^{-1} mol^{-1}, can reasonably be associated with the low-frequency modes that are not detected in this study by Raman spectroscopy and have only been taken into account here in an approximate way.

The LIESST experiments allowed us to study the kinetics of the HS → LS relaxation. The occurrence of two well-differentiated regimes has been evidenced by the thermal dependence of $k_{HL}(T)$. Thermal activation and quantum tunneling are the main processes accounting for the relaxation in the HT and LT regions, respectively. In the theory of nonadiabatic multiphonon relaxation,[28] the LT tunneling rate, k^o_{HL}, can be expressed as follows:

$$k^o_{HL} = \frac{2\pi}{\hbar^2 \omega} H_{HL}{}^2 g \frac{S_{HL}{}^p \exp(-S_{HL})}{p!} \qquad (11)$$

where H_{HL} is the electronic matrix element $H_{HL} = \langle \Phi_{HS} | H_{SO} | \Phi_{LS} \rangle$, which is estimated to be around 150 cm^{-1};[28] $g = 1$ is the electronic degeneracy of the final LS state. S_{HL} represents the Huang−Rhys factor, which is a measure of the horizontal displacement of the HS and LS wells,

$$S_{HL} = \frac{1}{2} f \frac{\Delta Q_{HL}{}^2}{\hbar \omega} \qquad (12)$$

where f, ΔQ_{HL}, and $\hbar\omega$ are the Fe−N bond force constant, the reduced coordinate change ($\Delta Q_{HL} = \sqrt{6}\Delta r_{HL}$) and the characteristic frequency of the [FeN_6] core, respectively.[30] The parameter p is the reduced energy gap, $\Delta E^o_{HL}/\hbar\omega$ between the two wells. It seems reasonable to consider, in a first approximation, that ΔH obtained from the calorimetric measurements, 644 cm^{-1} for **1**, is close to the corresponding ΔE^o_{HL}. Then, p can be estimated as 1.4 taking into account the $\hbar\omega$ value of 464 cm^{-1} obtained from the geometric average of the Raman spectral peak frequencies recorded for **2** at 110 K. Further, the value of $S_{HL} \approx 53$, can be graphically deduced from the expression (11) when the rate constant estimated at 10 K, $k_{HL}(LT) \approx 1 \times 10^{-6}$ s^{-1}, is considered. From this S_{HL} value, expression (12) leads to $\Delta r_{HL} \approx 0.17$ Å consistent with $f \approx 4.5 \times 10^5$ dyn cm^{-1}.

No direct comparison with a structural determination of Δr_{HL} can be made for **2** because of the crystal cracking at temperatures close to the spin transition. However, $\Delta r_{HL} = 0.17$ Å has been obtained for **1** (after 100% HS molar fraction correction at room temperature) from crystallographic studies and lends support to the above considerations.

Acknowledgment. We deeply thank Professor François Varret for very helpful discussions. We are grateful to the European Commision for financial support through the TMR-Network "Thermal and Optical Switching of Spin States (TOSS)", Contract No. ERB-FMRX-CT98-0199EEC/TMR. We thank the financial assistance from the Spanish DGICYT through Projects PB97-1397 and MAT97-0987, and the Programa de AccionesIntegradas Hispano-Francesas (HF1999-0091).

Supporting Information Available: Temperature dependence of ln(A_{tot}) data derived from the Mössbauer spectra of **1**. This material is available free of charge via the Internet at http://pubs.acs.org.

References and Notes

(1) (a) Universitat de València. (b) Laboratoire de Chimie de Coordination du CNRS, Toulouse. (c) Institut de la Matière Condensée de Bordeaux. (d) Universitat Politècnica de València. (e) School of Chemistry, Queen's University of Belfast. (f) CSIC−Universidad de Zaragoza.

(2) Lehn, J. M. *Supramolecular Chemistry*; VCH: Weinheim, 1995.

(3) Gütlich, P. *Struct. Bonding* **1981**, *44*, 83.

(4) E. König, E.; Ritter, G.; Kulshreshtha, S. K. *Chem. Rev.* **1985**, *85*, 219.

(5) König, E. *Prog. Inorg. Chem.* **1987**, *35*, 527.

(6) Sorai, M.; Seki, S. *J. Phys. Chem. Solids* **1974**, *35*, 555.

(7) (a) Lawthers, I.; McGarvey, J. J. *Chem. Commun.* **1982**, 906. (b) Lawthers, I.; McGarvey, J. J. *J. Am. Chem. Soc.* **1984**, *106*, 4280. (c) McGarvey, J. J.; Lawthers, I.; Heremans, K.; Toftlund, H. *Inorg. Chem* **1990**, *29*, 252.

(8) (a) Decurtins, S.; Gütlich, P.; Hasselbach, K. M.; Spiering, H.; Hauser, A. *Inorg. Chem.* **1985**, *24*, 2174. (b) Decurtins, S.; Gütlich, P.; Köhler, C. P.; Spiering, H.; Hauser, A. *Chem. Phys. Lett.* **1984**, *105*, 1.

(9) Beattie, J. K. *Adv. Inorg. Chem.* **1988**, *32*, 2.
(10) Xie, C. L.; Hendrickson, D. N. *J. Am. Chem. Soc.* **1987**, *109*, 6981.
(11) Hauser, A. *Chem. Phys. Lett.* **1992**, *192*, 65.
(12) O'Connor, C. J., Coronado, E., Delhaès, P., Gatteschi, D., Miller, J. S., Eds. *Molecular Magnetism: From Molecular Assemblies to the Devices*; NATO Adv. Stud. Inst. Ser. E, vol. 321; Klumer: Dordrecht, The Netherlands, 1996; p 521.
(13) Real, J. A.; Muñoz, M. C.; Faus, J.; Solans, X. *Inorg. Chem.* **1997**, *36*, 3008.
(14) Varret, F. *Procedings of the International Conference on Mössbauer Effect Applications*, Jaipur, India, 1981; Indian National Science Academy: New Delhi, 1982.
(15) Bell, S. E. J.; McGarvey, J. J.; Rigby, S. J.; Walmsley, D. G. J. *Raman Spectrosc.* **1991**, *22*, 767.
(16) (a) Adler, P.; Hauser, A.; Vefn, A.; Spiering, H.; Gütlich, P. *Hyperfine Interact.* **1989**, *47*, 343. (b) Adler, P.; Spiering, H.; Gütlich, P. *Chem. Phys. Lett.* **1994**, *226*, 289.
(17) Henry, M.; Teillet, J.; Varret, F. *Rev. Phys. Appl*. **1980**, *15*, 1095.
(18) (a) Boukheddaden, K.; Varret, F. *Hypefine Interact.* **1992**, *72*, 349. (b) Bousseksou, A. Ph.D. Thesis, Université Pierre et Marie-Curie, Paris, 1992. (c) Boinnard, D.; Bousseksou, A.; Dworkin, A.; Savariault, J−M.; Varret, F.; Tuchagues, J. P. *Inorg. Chem*. **1994**, 33, 271.
(19) Claude, R.; Real, J. A.; Zarembowitch, J.; Kahn, O.; Ouahab, L.; Grandjean, D.; Boukheddaden, K.; Varret, F.; Dworkin, A. *Inorg. Chem*. **1990**, *29*, 4442.
(20) Bousseksou, A.; McGarvey, J. J.; Varret, F.; Real, J. A.; Tuchagues, J. P.; Dennis, A. C.; Boillot, M. L. *Chem. Phys. Lett.* **2000**, *318*, 409.
(21) Bousseksou, A.; Nasser, J.; Linares, J.; Boukheddaden, K.; Varret, F. *J. Phys. 1 (Paris)* **1992**, *2*, 1381.
(22) Kazutoshi, K.; Sorai, M.; Konti, A. J.; Hendrickson, D. N. *J. Phys. Chem. Solids* **1993**, 54, 1621.
(23) Paulsen, H.; Winkler, H.; Trautwein, A. X.; Grünstendel, H.; Rusanov, V.; Toftlund, H. *Phys. Rev.* **1999**, *B 59*, 975.
(24) Bousseksou, A.; Constant−Machado, H.; Varret, F. *J. Phys. 1 (Fr.)* **1995**, *5*, 747, and references therein.
(25) Létard, J. F.; Guionneau, P.; Rabardel, L.; Howard, J. A. K.; Goeta, A. E.; Chasseau, D.; Kahn, O. *Inorg. Chem.* **1998**, *37*, 4432.
(26) Létard, J. F.; Capes, L.; Chastanet, G.; Moliner, N.; Létard, S.; Real, J. A.; Kahn, O. *Chem. Phys. Lett.* **1999**, *313*, 115.
(27) Hauser, A.; Gütlich, P.; Spiering, H. *Inorg. Chem.* **1986**, *25*, 4245.
(28) Buhks, E.; Navon, G.; Bixon, M.; Jortner, J. *J. Am. Chem. Soc.* **1980**, *102*, 2918.
(29) Slichter, C. P.; Drickamer, H. G. *J. Chem. Phys* **1972**, *56*, 2142.
(30) (a) Hauser, A.; Vef, A.; Adler, P. *J. Chem. Phys.* **1991**, *95*, 8710. (b) Hauser, A. *Coord. Chem. Rev.* **1991**, *111*, 275. (c) Hauser, A. *Comm. Inorg. Chem.* **1995**, *17*, 17. (d) Hauser, A.; Jeftic, J.; Romstedt, H.; Hinek, R.; Spiering, H.; Gütlich, P. *Coord. Chem. Rev.* **1999**, *190−192*, 471.